Tryptophan Dynamics and Structural Refinement in a Lipid Bilayer Environment: Solid State NMR of the Gramicidin Channel†

W. Hu,‡ N. D. Lazo,§ and T. A. Cross*

Center for Interdisciplinary Magnetic Resonance at the National High Magnetic Field Laboratory, Institute of Molecular Biophysics, and Department of Chemistry, Florida State University, Tallahassee, Florida 32306

Received July 17, 1995; Revised Manuscript Received September 8, 1995⊗

ABSTRACT: Tryptophans in the gramicidin channel are important for defining the conformation and the orientation with respect to the bilayer normal and for facilitating cation conductance. Here, high-resolution structure and dynamics of these rings are characterized by solid state NMR. Both oriented and unoriented lipid bilayer preparations are used. Fast frozen lipid bilayer preparations of unoriented samples have been used to obtain static characterizations of nuclear spin interaction tensors. The temperature dependence of these unoriented samples and the spectral features of fast frozen oriented samples were used to experimentally define the local motions of the individual indole rings. Local motions were shown to have amplitudes as high as ±29°, and the motions were dominated by libration about the χ_2 axis. The high-resolution structure has been achieved by interpreting seven precise (±0.3°) orientational constraints from ^2H and ^{15}N NMR for each indole ring in light of the motionally averaged interaction tensors. Each of the four indoles is restricted to a unique orientation of the ring with respect to the bilayer normal and one of two possible rotameric states. The side chain torsion angles for each residue are very similar, generating similar electric dipole moment orientations with respect to the channel.

High-resolution dynamic characterizations are critical for elucidating high-resolution protein structure and for a detailed understanding of protein function. This is true for the interpretation of NOE-derived[1] distance constraints and *J* coupling-derived torsional constraints from solution NMR, and it is also true for distance and orientational constraints derived from solid state NMR. For a lipid bilayer-bound polypeptide, the combined use of fast frozen preparations to avoid bilayer distortions and motional averaging of tensors can provide high-resolution dynamic characterizations. Here, these methods are refined and demonstrated using the monovalent cation-selective channel-forming polypeptide gramicidin A in hydrated lipid bilayers. More specifically, this study will focus on the functionally important tryptophan side chains of this channel.

Gramicidin is a mixture of polypeptides produced by *Bacillus brevis* during the transition from vegetative growth to sporulation. The amino acid sequence for the dominant species, gramicidin A, is HCO-Val_1-Gly_2-Ala_3-D-Leu_4-Ala_5-D-Val_6-Val_7-D-Val_8-Trp_9-D-Leu_{10}-Trp_{11}-D-Leu_{12}-Trp_{13}-D-Leu_{14}-Trp_{15}-$NHCH_2CH_2OH$. Both termini are blocked, and the polypeptide is very hydrophobic. Consequently, it is completely solubilized within the lipid bilayer in its channel form, where it has specificity for monovalent cations. The channel pore is lined with amide linkages of the polypeptide backbone, and the side chains radiate toward the lipid environment. To form a 4 Å diameter pore, 6.3 residues per turn are used in a single-stranded helix (Urry, 1971). The helical sense is right-handed (Nicholson & Cross, 1989), and more recently, the backbone structure has been experimentally defined at high resolution in a lipid bilayer by solid state NMR (Ketchem et al., 1993). Several initial attempts to characterize the indole conformations have been published (Cornell et al., 1988; Separovic et al., 1991; Killian et al., 1992; Hu et al., 1993; Koeppe et al., 1994, 1995); most of these efforts were based on assumed structural models for the polypeptide backbone, using few structural constraints for the side chains, and none of them had well-characterized tensors for the interpretation of the orientational constraints. These tryptophans are fundamentally important to both the structure and function of the channel. On the basis of the structure, the indole NH groups appear to hydrogen bond to the bilayer surface (Takeuchi et al., 1990; Hu et al., 1993; Ketchem et al., 1993; Hu & Cross 1995), thereby orienting the channel with respect to the surface and inducing the transition from double-stranded to single-stranded helices (Zhang et al., 1992; Arumugam et al., 1995). Moreover, this hydrogen bond formation to the bilayer surface appears to be a primary cause for the right-handed helical sense of the channel (W. Hu, M. Cotten, and T. A. Cross, unpublished results). Second, the indole dipole moments are aligned so as to lower the potential energy barrier at the bilayer center for conductance of the cations (Becker et al., 1991; Hu et al. 1993; Hu & Cross, 1995).

Many proteins and polypeptides exist in anisotropic environments that have proven to be very difficult to study by standard methods for structure determination. Solid state NMR spectroscopy requires samples that do not have isotropic global motions, and so it is very appropriate for such studies (Cross, 1994; Cross & Opella, 1994). Furthermore, only when the global motions do not dominate the NMR observables (such as relaxation times for solution or solid state NMR) can the local motions be characterized with considerable accuracy. In solution NMR, the anisotropy of all nuclear spin interactions is averaged to isotropic values

† This work has been supported by the National Science Foundation (DMB-9317111) and the National High Magnetic Field Laboratory.

‡ Present address: Biophysics Research Division, University of Michigan, 930 North University, Ann Arbor, MI 48109-1055.

§ Present address: Department of Dermatology, College of Medicine, University of Iowa, Iowa City, IA 52242.

⊗ Abstract published in *Advance ACS Abstracts,* October 15, 1995.

[1] Abbreviations: DMPC, dimyristoylphosphatidylcholine; HPLC, high-performance liquid chromatography; QCC, quadrupole coupling constant; DCC, dipole coupling constant; rms, root mean square; rmsd, root mean square deviation; NOE, nuclear Overhauser effect; gA, gramicidin A.

0006-2960/95/0434-14138$09.00/0 © 1995 American Chemical Society

by global motions and relaxation is induced primarily by the influence of global rather than local motions. On the contrary, proteins and polypeptides in anisotropic environments display residual anisotropic nuclear spin interaction tensors, such that local motions can be readily detected.

To relate the observation of residual anisotropies to the molecular frame, it is necessary to know how the spin interaction tensor is oriented in the molecular frame. For dipolar and quadrupolar interactions, the orientation of the unique tensor elements can be safely assumed to be along the internuclear vector. Moreover, with an accurate determination of the internuclear bond length, it is possible to calculate the dipolar magnitude. With its orientation known and its magnitude calculable, the dipolar interactions are very attractive for structural studies. Carbon-bound ^{2}H has a very small asymmetry, and its unique tensor element is closely aligned to the internuclear vector. While the static magnitude of these quadrupolar interactions cannot be calculated accurately, they have been experimentally determined from model compounds below 200 K (Kinsey et al., 1981).

By observing the chemical shift powder pattern directly, the tensor element magnitudes can be determined for the site, molecule, and environment of interest. Tensor element orientations have more typically been determined from single crystal studies of model compounds. Such a characterization will be qualitatively useful for a class of related compounds; however, characterization of the relative orientation of nuclear spin interaction tensors has proven to be quantitatively the most accurate approach (Hiyama et al., 1988; Teng et al., 1992).

Such chemical shift tensor characterizations have been difficult to achieve in a lipid environment because a dry lipid environment may not represent a close approximation to a bilayer environment, and in the presence of water, there exist both local and global motions of significant amplitude. The global motions have been characterized in detail as a function of temperature by monitoring the intermediate exchange rate averaging of the Ala_3- and Ala_5-deuterated methyl groups (Lee et al., 1993; North & Cross, 1995). Furthermore, when the sample temperature is lowered below the gel to liquid–crystalline phase transition of the lipids, the bilayers can become significantly distorted, resulting in small conformational changes for the polypeptide or protein (Nicholson et al., 1991). Hence, fast frozen samples are used which avoids bilayer distortions and large ice crystal formation (Evans et al., 1993) that can further distort the polypeptide environment if not its structure directly. Furthermore, when observed below 200 K, no significant librational motion occurs and the vibrational amplitudes are small, resulting in the observation of static spectra for the site of interest in the environment of interest. With such procedures, it has been possible to achieve accurate tensor orientations for backbone amide sites via a dipolar-coupled chemical shift powder pattern (Lazo et al., 1995). For the indole studies reported here, the chemical shift tensor orientations have been assumed from model compounds rather than by direct observation, due to a lack of an appropriate dipolar coupling (Hu et al., 1993). However, the fast freezing methods have been essential for the characterization of the static tensor element magnitudes for specific sites in gramicidin A in fully hydrated lipid bilayers.

Once the tensors are defined in the molecular frame, it is possible to interpret residual anisotropies to achieve a detailed assessment of dynamics. Previously, a number of papers have been published on the 180° flip motion of phenylalanine and tyrosine (Kinsey et al., 1981; Torchia, 1984; Gall et al., 1982; Frey et al., 1985). Such motions result in unique line shapes. It has been recognized in several of these studies that the width of the residual anisotropy is less than that predicted by the averaging of the flip or rotational motions alone. Hence, the effects of librational motions have been observed, and in a few cases, the spectra have been simulated with an assumed motional model. For polypeptides or proteins with global motions that are fast on the nuclear spin interaction time scale, this analysis becomes further complicated, since the residual anisotropy is dependent on the orientation of the interaction tensor to the global motional axis; i.e., the separation of structural and dynamic effects on the anisotropy becomes very challenging. However, with the fast frozen preparations, it is possible to monitor the residual anisotropy as the temperature is raised from a static state to the temperature where global motions are induced (approximately 10°C; Lee et al., 1993). In this way, effects of global and local motions can be separated. It will be demonstrated here that an analysis of the residual anisotropy can yield a description of the axis of librational motions in the molecular frame as well as the amplitude. Consequently, anisotropic rather than isotropic librational motions will be characterized. In addition, uniformly aligned preparations that display a range of orientations for a given site reflecting the librational amplitude at room temperature can be fast frozen. These two independent approaches have provided consistent results for each of the indole side chains in hydrated lipid bilayer preparations of the gramicidin channel.

With well-defined motionally averaged tensors, it is possible to refine the set of side chain torsion angles on the basis of orientational constraints for the tryptophan residues. Previously, there have been ambiguities in the assignment of the ^{2}H quadrupolar constraints to specific sites in the Trp_9-d_5 indole ring. With well-characterized tensors, it is here possible to achieve a unique assignment for these constraints.

METHODS AND MATERIALS

Isotopically labeled amino acids were purchased from Cambridge Isotope Laboratories. Dimyristoylphosphatidylcholine (DMPC) was purchased from Sigma at +99% and was used without further purification. The 9-fluorenylmethoxycarbonyl blocking chemistry and peptide synthesis on a model 430A Applied Biosystems peptide synthesizer were performed as described previously (Fields et al., 1988; Fields et al., 1989). Peptides were greater than 98% pure upon cleavage from the resin and were used without further purification.

Unoriented samples of gramicidin in hydrated lipid bilayers were prepared by cosolubilizing the peptide and lipid in 95% benzene/5% ethanol. The solution was frozen in liquid nitrogen and lyophilized to produce a powder, which was then hydrated with 40% (volume/total weight) HPLC-grade water. The samples were incubated for at least 2 weeks at 45 °C after centrifugation for 15 min at 2000g. Fast freezing was achieved by plunging thin films of this bilayer preparation into liquid propane precooled to 85 K. The frozen films were transferred to a glass tube submersed in liquid nitrogen. Once the entire sample had been transferred, the tube was sealed and transported to the precooled solid state NMR probe for observation.

Oriented samples were prepared by spreading the cosolubilized peptide and lipid described above onto 25 glass

coverslips cut to 5.8 mm by 18 mm. The solvent was removed at room temperature and further dried under vacuum. The coverslips and sample were stacked into a square glass tube (6 × 6 × 20 mm) and then hydrated with 50% (volume/total weight) HPLC-grade water before the tube was sealed. The sample usually became transparent and uniformly oriented after approximately 2 weeks at 45°C. Fast frozen oriented samples were prepared by spreading the cosolubilized sample on 15 glass coverslips (7.5 × 18 mm). After the sample was completely dried, 5 μL of HPLC-grade water was added to each coverslip and the sample was covered with a clean coverslip. These individual films were incubated for 3 weeks in a water-saturated atmosphere until the samples became transparent. The films sandwiched between coverslips were plunged into liquid propane and stacked in a square sample tube (8 × 8 × 20 mm) that was cooled in liquid nitrogen. The sample tube was then sealed and transferred to the precooled NMR probe.

The ^{15}N and ^{2}H NMR experiments were performed on a spectrometer assembled around an Oxford Instruments 400/89 superconducting magnet and a Chemagnetics data acquisition system. The low-temperature experiments were performed as described by Lazo et al. (1993, 1995). ^{15}N spectra were obtained at 40.6 MHz with cross-polarization and ^{1}H dipolar decoupling. Typical parameters used were 6 μs 90° pulse widths, 1 ms mixing time, and a 7 s recycle delay. For powder pattern spectra, a Hahn echo was often used with minimal pulse intervals to avoid acoustic ringing. The ^{15}N spectra are referenced either to a saturated solution of $^{15}NH_4NO_3$ or to the isotropic frequency of the chemical shift tensor. This later referencing is done to avoid the temperature dependence of the isotropic frequencies. ^{2}H NMR spectra were obtained at 61.5 MHz using the standard quadrupole echo pulse sequence. Typical parameters for data acquisition included a 1 MHz sweep width, 2.8 μs 90° pulse width, 30 μs echo delays, and either a 0.5 or 1.0 s recycle delay.

All the NMR spectra were processed on a Silicon Graphics workstation using Felix software. Molecular modeling was performed using Insight II software. Calculations and simulations of spectra were carried out on either a Sun Sparc workstation or the Silicon Graphics workstation using software packages developed in the laboratory, such as TENSORI for the powder pattern line shapes and TORC for the torsion angle calculations.

RESULTS

Shown in Figure 1 is a range of ^{15}N NMR data that can be used to characterize the dynamics of a macromolecular site. All spectra for this effort were obtained from fully hydrated lipid (DMPC) bilayer preparations containing gramicidin with a single amino acid isotopically labeled. Here [$^{15}N_{\epsilon 1}$-Trp$_9$]gramicidin has been observed in unoriented (A and B) and oriented samples (C and D). The spectrum in Figure 1B shows that motions of the channel substantially average the chemical shift anisotropy when samples are above the gel to liquid−crystalline phase transition temperature. The static spectrum of the anisotropy shown in Figure 1A has been obtained from a fast frozen unoriented sample observed at 143 K. Without fast freezing, the discontinuities are not well-defined due to heterogeneous broadening, and hence, it is difficult to accurately define the magnitude of the tensor elements.

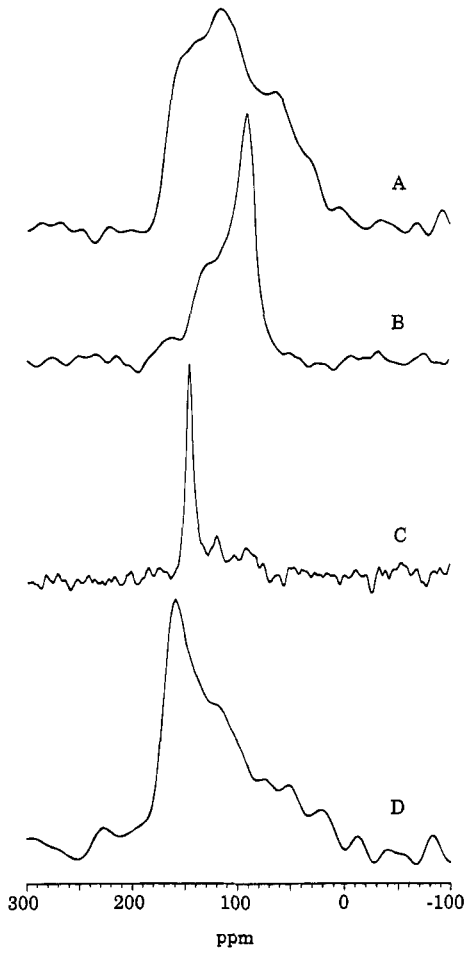

FIGURE 1: ^{15}N NMR spectra of [$^{15}N_{\epsilon 1}$-Trp$_9$]gramicidin A in fully hydrated bilayers of DMPC. (A) Spectrum obtained at 143 K with 2400 acquisitions of an unoriented sample prepared by fast freezing techniques. This represents the static chemical shift tensor. (B) Spectrum of an unoriented sample obtained at room temperature (above the gel to liquid crystalline phase transition) with 896 acquisitions. The motional averaging that results in this axially symmetric line shape is due to the global rotation of the channel about its helical axis. (C) Spectrum obtained with 8900 acquisitions of a sample oriented such that the bilayer normal is parallel with respect to the magnetic field. The single sharp resonance represents a unique orientation of this indole with respect to the channel axis. (D) Spectrum of a fast frozen oriented sample obtained with 2400 acquisitions. The broadening is due to orientational dispersion resulting from the rapid loss of motional freedom and considerable powder pattern intensity from unoriented polypeptide.

Samples that are oriented with respect to the magnetic field result in narrow resonances (Figure 1C). Because the axial rotation of the channel is parallel to the bilayer normal and because the bilayer normal has been aligned parallel to the magnetic field, the observed chemical shift occurs at the $\sigma_{\parallel}$ frequency of the axially symmetric powder pattern observed in Figure 1B. When an oriented sample is fast frozen and observed at 143 K, the resonance broadens for two reasons. First, such samples have considerable unoriented domains that give rise to a static powder pattern, as in Figure 1A. Second, local librations, as well as axial global motions, cease at temperatures below 200 K, resulting in a range of orientations for the site of interest. This orientational range results in a range of chemical shifts, such that the intensity distribution reflects the orientational range associated with the librational motions at room temperature.

However, for the effort here, the primary mechanism for deriving the motional characteristics is to study the line shapes of unoriented samples at temperatures below the gel

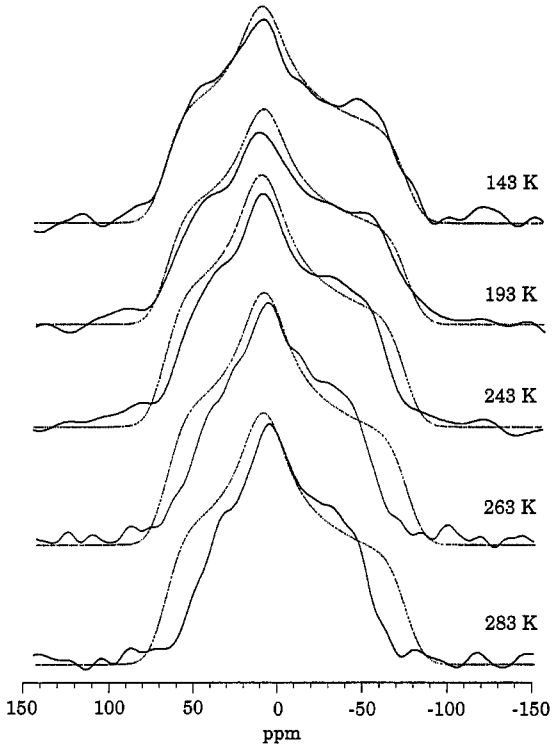

FIGURE 2: ^{15}N NMR spectra of unoriented samples of [$^{15}N_{\epsilon 1}$-Trp$_{11}$]-gramicidin A in fully hydrated lipid bilayers. Samples were fast frozen and allowed to warm to the temperature indicated for observation with between 2000 and 6400 acquisitions. One hour for equilibration was allowed prior to recording the data. The dotted line is the simulation of the experimental spectrum at 143 K. As the temperature increases, the tensor elements are averaged by anisotropic local librational motions.

to liquid−crystalline phase transition temperature. In Figure 2, a fast frozen sample has been observed at 143 K and at a variety of temperatures up to 10 °C, a temperature just below the onset of global axial rotation (Lee et al., 1993). Between 200 and 283 K, considerable averaging of the powder pattern occurs. In this figure, the spectral simulation (dotted line) shown with each experimental spectrum is the simulation of the spectrum obtained at 143 K. In this way, the differences between the static and motionally averaged

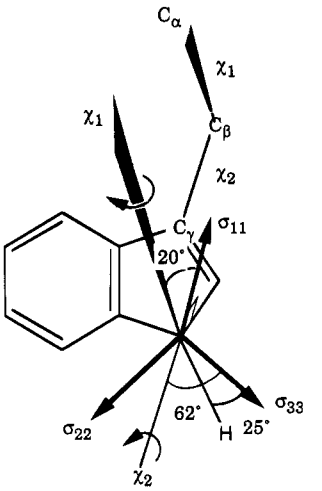

FIGURE 3: Orientation of the $^{15}N_{\epsilon 1}$ chemical shift tensor elements with respect to the molecular frame as determined from $^{2}H-^{15}N$ dipolar-coupled ^{15}N chemical shift powder pattern spectra of the amino acid (Hu et al., 1993). σ_{11} is perpendicular to the indole ring plane, and the σ_{33} element makes an angle of 25° with respect to the N−H bond and an angle of 62° with respect to the χ_2 axis. For the rotameric χ_2 state of 270°, the angle between χ_1 and σ_{11} is approximately 20°.

spectra are emphasized. Furthermore, it is clear that the librational motion is anisotropic. The σ_{22} element is essentially unaffected, while the σ_{11} and σ_{33} elements are considerably reduced in magnitude. Because the chemical shift tensor has a fixed orientation with respect to the molecular frame, it is possible to determine the approximate axis in the molecular frame about which the motions are occurring. In other words, the tensor element that is least averaged by the dynamics lies closest to the axis of molecular motion. The orientation of this tensor with respect to the molecular frame (Figure 3) has previously been determined by aligning it with respect to the $^{15}N-^{2}H$ dipolar interaction tensor which has its unique axis parallel to the internuclear vector (Hu et al., 1993). The σ_{22} vector is the tensor element closest to the χ_2 axis, suggesting that the librational motion may be occurring predominantly about the χ_2 torsion angle, since σ_{22} is essentially unaffected by the molecular motions.

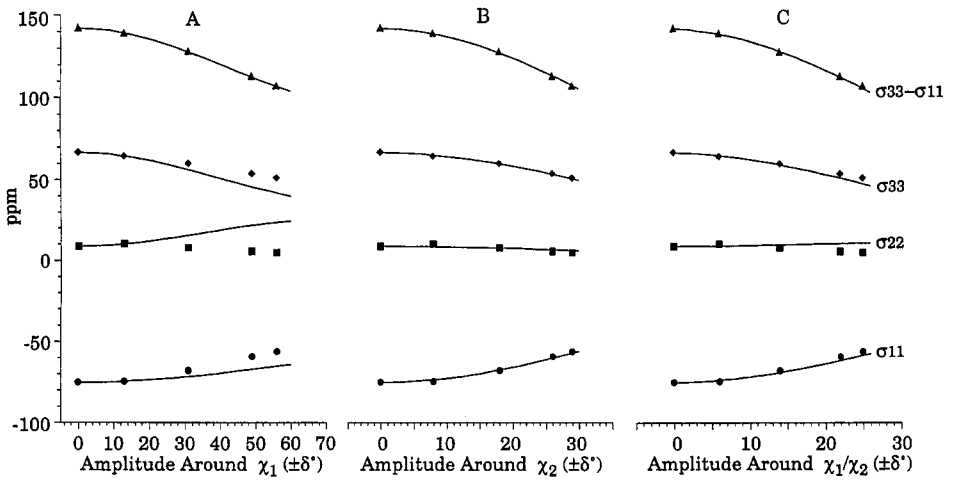

FIGURE 4: Variable-temperature data of Figure 2 analyzed in light of three models for the librational motion of the Trp$_9$ side chain. For each model, the anisotropy (▲, given by $\sigma_{33} - \sigma_{11}$) as a function of temperature (143, 193, 243, 263, and 283 K) is fit by adjusting the librational amplitude to achieve agreement with the experimental result. (A) Librations are restricted to the χ_1 torsion angle with a fixed χ_2 angle of 270°. Such librations do not average the σ_{11} (●) element enough and average the σ_{22} (■) and σ_{33} (◆) elements too much. (B) Librations are restricted to the χ_2 axis. The fit to the individual tensor elements is very good, and it is achieved without such large librational amplitudes as suggested by the analysis in part A. (C) Equal amplitudes for librational motions exist about the χ_1 and χ_2 axes. The averaging of the tensor elements is not as well fit with this model as it is with the χ_2 motion alone.

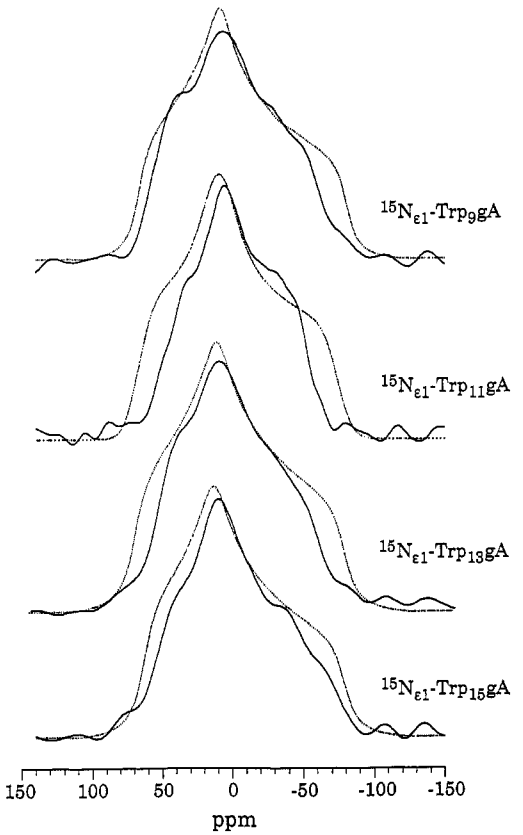

FIGURE 5: ^{15}N NMR powder pattern spectra obtained at 283 K (solid line) and compared to the simulation of the static spectrum at 143 K (dashed line) for each of the indole rings. The spectra are similar to those in Figure 2 and were obtained with between 2400 and 8600 acquisitions, showing that the averaging of the tensor elements for each indole is similar. σ_{22} is averaged very little, while σ_{11} and σ_{33} are averaged to differing extents, representing somewhat different librational amplitudes for the four sites.

Table 1: Librational Amplitude Characterization

	Trp$_9$	Trp$_{11}$	Trp$_{13}$	Trp$_{15}$
powder pattern averaging[a]	22°	29°	25°	19°
orientational dispersion[b]	25°	26°	26°	19°

[a] Assessed from unoriented samples at 283 K. [b] Assessed from oriented samples at 143 K.

Figure 4 shows the best fit to the magnitude of the residual anisotropy at each temperature using three different librational models. Neither motions about the χ_1 axis alone nor equal amplitudes for the motion about the χ_1 and χ_2 axes resulted in reasonable fits to the anisotropy. In other words, while the magnitude ($\sigma_{33} - \sigma_{11}$) could be fit by each model, the exact values of σ_{ii} were not simultaneously fit. However, motions about the χ_2 axis alone fit all of the data very well. This does not exhaust the possible models, but it shows that the predominant motions are about the χ_2 axis. Data for the other tryptophan sites (Figure 5) yield similar results, although amplitudes for the librations vary somewhat as shown in Table 1. In all cases, the anisotropic motions are consistent with the predominant motion occurring about the χ_2 axis. In Table 2, the static chemical shift tensor elements are summarized.

To complement these dynamic characterizations, fast frozen oriented sample preparations have been studied (Figure 6A). Such samples which are prepared using individual pairs of glass plates that are plunged into liquid propane are not as well-aligned as our typical samples (Figure 6C). The amount of unoriented sample in the fast frozen preparations can be determined by subtracting powder pattern line shapes obtained at room temperature (such as those shown in Figure 1B) for each specific site studied. Therefore, the motionally averaged line shape parameters (reported in Table 2) are not variables in fitting spectra, such as these in Figure 6A where there is a mixture of oriented and unoriented bilayers. The powder pattern intensity or percent of unoriented material in each preparation is a variable that can be readily estimated, and the powder pattern can be subtracted from the spectra as in Figure 6B.

When the fast frozen samples are observed at 143 K (Figure 7A), static powder patterns can be subtracted without evaluating any variables. Again, the tensor element magnitudes are known from spectra such as those shown in Figure 1A, and the powder pattern intensity determined at room temperature (Figure 6B) is used without modification

Table 2: Chemical Shift Tensor Characterization[a]

	Trp$_9$	Trp$_{11}$	Trp$_{13}$	Trp$_{15}$
static[b]				
σ_{11}	-79 ± 4	-75 ± 3	-79 ± 3	-78 ± 4
σ_{22}	11 ± 3	9 ± 3	11 ± 3	14 ± 3
σ_{33}	68 ± 3	67 ± 3	69 ± 3	64 ± 3
with global and local motions[c]				
$\sigma_{\parallel}$	39 ± 2	38 ± 2	38 ± 2	34 ± 2
$\sigma_{\perp}$	-20 ± 2	-19 ± 2	-19 ± 2	-17 ± 2
σ_{iso}[d]	107 ± 2	108 ± 2	108 ± 2	109 ± 2

[a] Tensor element values reported relative to $\sigma_{iso} = 0$ ppm. [b] Assessed from hydrated samples at 143 K. [c] Assessed from hydrated samples at room temperature. [d] Relative to saturated $^{15}NH_4NO_3$ solution at 0 ppm.

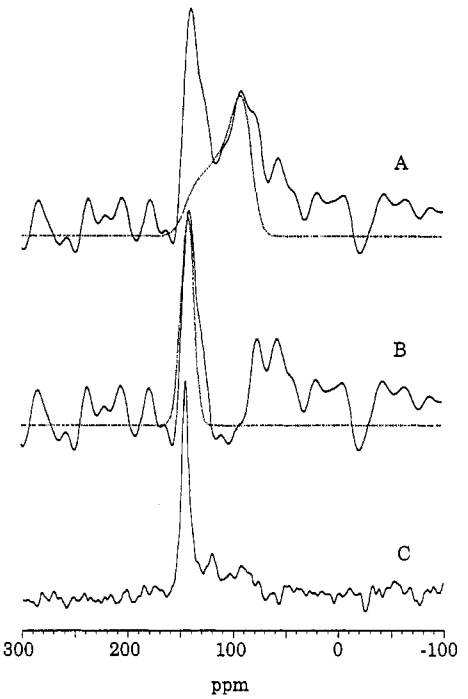

FIGURE 6: ^{15}N NMR spectra of [$^{15}N_{\epsilon 1}$-Trp$_9$]gramicidin A in oriented lipid bilayers observed at room temperature. (A) Sample that has been fast frozen prior to observation with 4700 acquisitions. The percentage of sample that is not oriented can be assessed through simulation of the line shape for which the powder pattern anisotropy is defined from spectra such as that in Figure 1B. (B) Spectrum as in part A with the powder pattern intensity subtracted. The line width of the residual intensity is considerably greater than that observed in the standard oriented samples, such as that shown in part C, which is reproduced from Figure 1C.

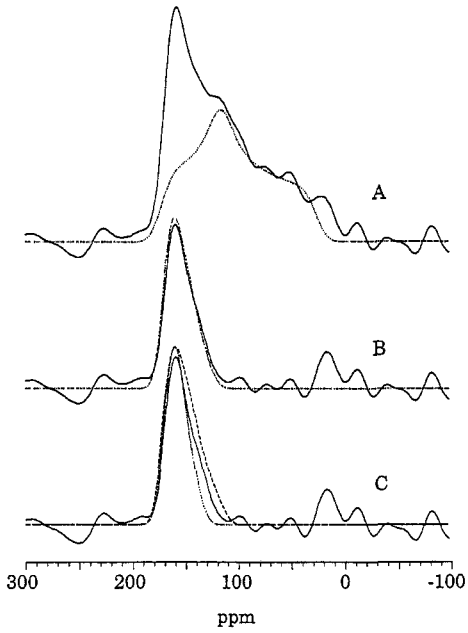

FIGURE 7: Processing of the ^{15}N NMR spectrum of fast frozen oriented bilayer preparations of [^{15}N-Trp$_9$]gramicidin A obtained at 143 K with 2400 acquisitions. (A) Considerable powder pattern intensity obscures the intensity from the aligned domains. The fraction of sample that is unoriented has been determined from Figure 6A, and the static tensor elements have been determined from spectra such as that in Figure 2. Therefore, the powder pattern intensity can be subtracted without assessing any additional variables. (B) Spectrum as in part A with the powder pattern subtracted. Spectral simulation using a χ_2 motional model suggests that the librational amplitude is 25°. (C) Spectral simulations of 20 and 30° librational amplitudes superimposed on the spectrum from part B.

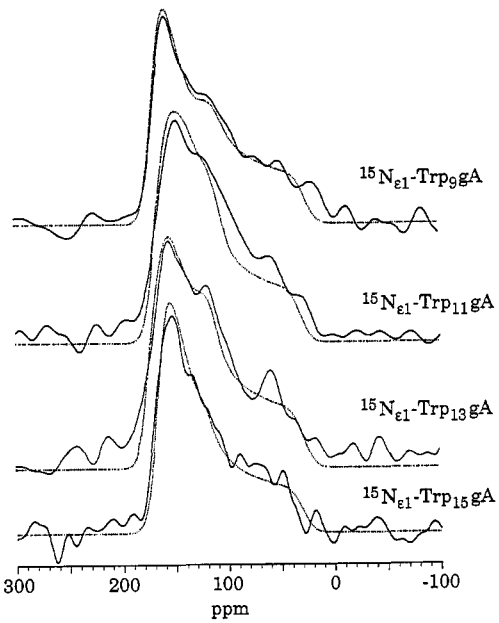

FIGURE 8: ^{15}N NMR spectra of fast frozen oriented bilayer preparations of [^{15}N-Trp]gramicidin A obtained at 143 K with 2400–5300 acquisitions. Spectra for Trp$_{11}$, Trp$_{13}$, and Trp$_{15}$ are compared to those for Trp$_9$. Spectral simulations represent the sum of the static powder pattern intensity plus the librationally broadened signal from the aligned domains of the sample.

at these low temperatures; therefore, all of the necessary parameters are defined. With the powder pattern intensity subtracted, the spectra can be simulated by assuming an orientational dispersion about the mean χ_2 torsional angle. This results in an asymmetric line shape (Figure 7B)

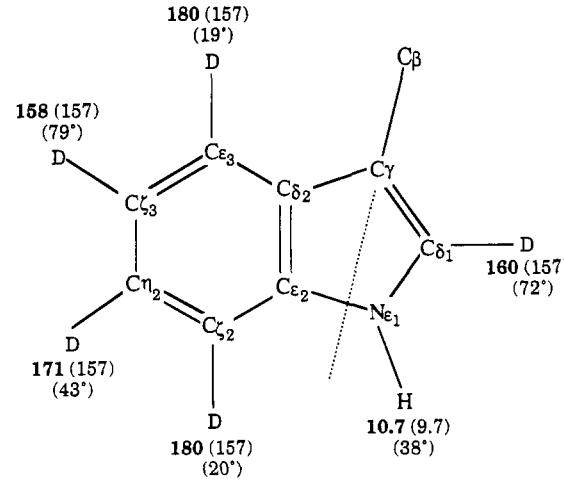

FIGURE 9: Anisotropic librational averaging of the nuclear spin interaction tensors in the indole ring of Trp$_9$. The number of degrees represents the angle of the unique tensor element, the C–H or N–H bond, to the χ_2 motional axis. The number in boldface represents the motionally averaged interaction magnitude; for the deuterated sites, it is the motionally averaged QCC, and for the indole N–H, it is the motionally averaged dipolar interaction. Next to the boldface numbers are prior estimates of the motionally averaged tensor elements, assuming an isotropic model for the librational motions.

Table 3: Motionally Averaged Dipolar and Quadrupolar Tensor Elements

	Trp$_9$	Trp$_{11}$	Trp$_{13}$	Trp$_{15}$
^2H QCC (static value = 183 kHz)				
$C_{\delta 1}$	160	146	154	165
$C_{\epsilon 3}$	180	178	179	181
$C_{\zeta 2}$	180	178	179	181
$C_{\zeta 3}$	158	144	152	164
$C_{\eta 2}$	171	163	167	173
$^{15}N-^1H$ DCC (static value = 11.3 kHz)				
$N_{\epsilon 1}$	10.7	10.3	10.6	10.9

calculated from a Gaussian distribution of orientations represented by an orientational half-width distribution of 25° for Trp$_9$. Shown in Figure 7C are two additional simulations spanning an orientational range from 20 to 30° clearly defining a range that is greater than the error for this dynamic amplitude characterization. The simulations of the entire line shape for each tryptophan are shown in Figure 8. The librational amplitudes determined in this way confirm the powder pattern averaging results tabulated in Table 1.

With the dynamics so precisely characterized, it is now possible to more accurately interpret the orientational constraints for the structural characterization of the tryptophan side chains. Shown in Figure 9 are the motionally averaged values of the quadrupole coupling constants (QCC) based on the powder pattern averaging results that characterized both an axis for the motion and an amplitude. The angle of each internuclear vector with respect to the motional axis is also shown. Furthermore, these values are compared to QCC values assuming an isotropic librational motion, i.e., equal amplitudes about each of three orthogonal axes, and therefore, the QCC for each internuclear vector is the same. Also presented in Figure 9 are similar calculations for the $^{15}N-^1H$ dipolar interaction, and these numbers are reported in Table 3 for each of the indoles.

The complete set of ^2H quadrupole splittings from oriented samples for each of the tryptophans is shown in Figure 10 and tabulated in Table 4. The narrowest line widths indicate a maximum mosaic spread of ±0.3°. Consequently, these

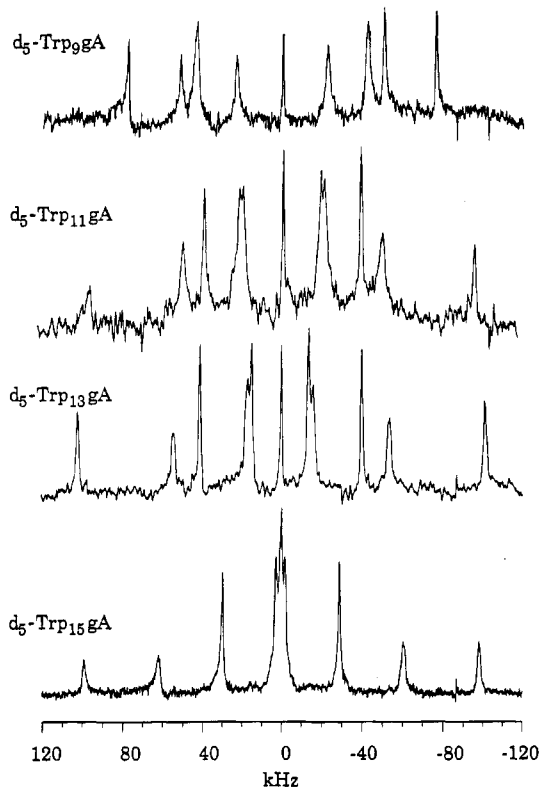

FIGURE 10: ^{2}H NMR spectra of Trp-d_5 labeled gramicidin A in uniformly aligned bilayers at room temperature. For Trp$_{11}$, Trp$_{13}$, Trp$_{15}$, five quadrupolar splittings can be identified. For Trp$_9$, only four splittings can be absolutely identified, although the splitting at 85 kHz appears to represent two resonances. These sharp resonances yield very high resolution orientational constraints and document the small mosaic spread (±0.3°) for the orientation of the channel with respect to the magnetic field.

Table 4: Orientational Constraints for the Indole Rings in the Gramicidin Channel

	Trp$_9$	Trp$_{11}$	Trp$_{13}$	Trp$_{15}$
^{2}H splitting (kHz)				
$C_{\delta 1}$	46	77	108	123
$C_{\epsilon 3}$	87	43	32	4
$C_{\zeta 2}$	85	39	28	1
$C_{\zeta 3}$	155	192	204	198
$C_{\eta 2}$	−102	−99	−81	−59
^{15}N−^{1}H splitting (kHz)				
$N_{\epsilon 1}$	13.2	11.1	10.1	7.7
^{15}N chemical shift (ppm; converted to $\sigma_{iso} = 0$ ppm)				
σ_{obs}	38	36	36	30

resonances represent a very precise set of constraints, and now with accurate motional characteristics for each deuterated site, these resonances are also accurate constraints. The entire set of ^{15}N and ^{2}H constraints can be analyzed to yield χ_1/χ_2 plots as shown in Figure 11, in which the minimum root mean square (rms) deviation between predicted and observed constraints is calculated. For Trp$_{11}$, Trp$_{13}$, and Trp$_{15}$, five quadrupolar splittings are defined from the observed spectra. From these sets of quadrupolar splittings, the $C_{\epsilon 3}/C_{\zeta 2}$ resonances are readily assigned to the splittings that are virtually identical. The remaining assignments are uniquely defined by a consideration of the ^{15}N−^{1}H dipolar interaction and the ^{15}N chemical shift constraint. This set of assignments leads to reasonable rms deviations between observed and predicted values as the χ_1 and χ_2 conformational space is completely searched. Furthermore, only one set of signs for the quadrupolar splittings yields reasonable rms

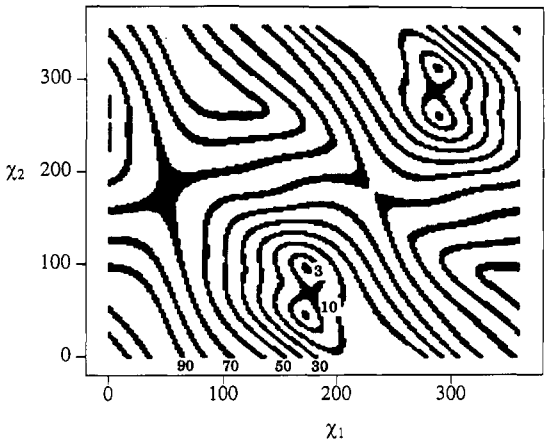

FIGURE 11: Contour plot of the minimal rmsd between the observed orientational constraints (quadrupolar, dipolar, and chemical shift) and the calculated observables based on the χ_1 and χ_2 torsion angles for the Trp$_9$ side chain and the experimentally defined backbone structure of the channel in a bilayer environment (Ketchem et al., 1993). The rmsd values for the contours are labeled in the figure. The four solutions fall within two rotameric states of the χ_1 and χ_2 torsion angles.

Table 5: χ_1/χ_2 Torsion Angle Solution Sets for the Gramicidin Channel Indoles

	Trp$_9$	Trp$_{11}$	Trp$_{13}$	Trp$_{15}$
χ_1	288	290	297	302
χ_2	263	279	270	264
χ_2	314	308	311	312
χ_1	174	171	169	165
χ_2	97	81	90	96
χ_2	46	52	49	48

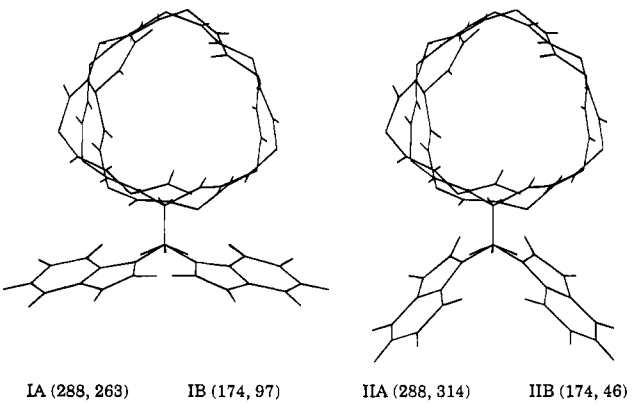

FIGURE 12: Four possible conformational states for Trp$_9$. All have the same orientation of the indole ring with respect to the channel axis and the magnetic field direction. Since the solid state NMR constraints are with respect to this one axis, the remaining ambiguities are not surprising. The conclusion from the orientational constraints is a unique orientation of the indole ring with respect to the channel axis. A similar conclusion is achieved for the other indole rings.

deviations. This analysis results in four well-defined minima with rmsd boundaries between the minima that are much greater than the experimental error, and hence, the native conformation lies in one of the minima, not somewhere between minima. These minima represent a precisely determined time-averaged conformational solution set (Table 5). Furthermore, the contours are not defined by energy terms, and hence, the dynamics for these sites (e.g., ±19° for Trp$_{15}$) does not suggest transitions between minima. All minima result in the same orientation of the ring with respect to the bilayer normal and the magnetic field direction as shown in Figure 12.

Table 6: Potential Trp_9 ^2H Splitting Assignments[a]

		splitting (kHz)	orientation (deg)	RMSD (deg)	χ_1 (deg)	χ_2 (deg)
		assignment options				
1[b]	$C_{\epsilon 3}/C_{\zeta 2}$	87/85	138/43	2.9	174	97, 46
					288	263, 314
2	$C_{\epsilon 3}/C_{\zeta 2}$	46/46	132/48	3.5	170	98, 49
	$C_{\delta 1}$	87	41		292	262, 311
3	$C_{\epsilon 3}/C_{\zeta 2}$	102/102	140/40	4.7	174	96, 47
	$C_{\zeta 3}$	−87	110		288	264, 313
4[c]	$C_{\epsilon 3}/C_{\zeta 2}$	152/152	147/33	4.3	196	92, 18
					266	268, 342

[a] Four possible assignments for the $C_{\epsilon 3}/C_{\zeta 2}$ deuterons corresponding to specific C−D bond orientations and four possible χ_1/χ_2 solutions for each assignment are possible. [b] This is the assignment used by Hu et al., 1993. [c] This is the assignment used by Koeppe et al., 1994.

For Trp_9, only four quadrupolar splittings are observed, and therefore, the assignment problem is further complicated by the assignment of the fifth splitting to one of the four observed signals. Two different values for this fifth splitting have been published (Hu et al., 1993; Koeppe et al., 1994), and additional solutions (Table 6) are consistent with the known covalent geometry of the indole ring (Subramanian & Sahayamary, 1989). Remarkably, a reasonable fit between experimental and predicted results (from a refined indole orientation) can be achieved for each of these possibilities. Our previously published assignment of the $C_{\epsilon 3}/C_{\zeta 2}$ resonances to the 87/85 kHz splitting yields the lowest rmsd between experimental and predicted orientation for all of the orientational constraints. Moreover, this 87/85 kHz splitting is the most intense resonance, further supporting the assignment of these two deuterons to this splitting. These rmsd results using the high-resolution dynamic characterizations and the ^{15}N data, as well as the ^2H results, generate an assignment for the fifth splitting of 85 kHz. With this unique assignment achieved, four possible torsion angle solutions are obtained, as with the other indole rings (Table 5).

DISCUSSION

While large amplitude local motions, such as ring flips or other jumps between rotameric states, have been characterized in detail by solid state NMR, motions within rotameric states have been poorly defined. By relaxation studies, small amplitudes have been modeled as a wobbling in a cone (London, 1980) or not modeled as in the model-free approach (Lipari & Szabo, 1982), but here it has been possible to experimentally characterize the motional model for the indole side chains. In this way, both the axis about which the local motions occur and the amplitude of the motions have been characterized. Furthermore, two independent approaches for obtaining the experimental data have resulted in very similar amplitudes. Both of these solid state NMR methods have been dependent on fast freezing the model membrane samples, prepared with 50% by weight water. Conformational heterogeneity, due to the gel to liquid−crystalline phase transition of the lipids and large ice crystal formation in the samples that leads to severe broadening of the resonances and a resultant loss of line shape detail, has been minimized by fast freezing.

Dynamics are very important in gramicidin. Recent studies have shown that there is coincidence in the time frame for the backbone librational motions and the kinetic rate at which cations translate from one carbonyl cluster to the next along the axis of the channel (North & Cross, 1993, 1995).

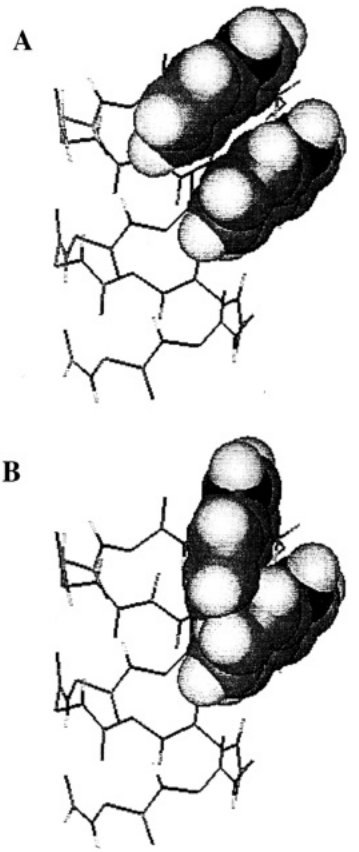

FIGURE 13: If Trp_9 and Trp_{15} are in a stacked conformation [see Hu and Cross 1995)], the characterized librational amplitudes of these rings suggest that the motions are coherent. The torsion angles for this display represent the mean conformational state plus/minus the librational amplitude about χ_2. (A) χ_1/χ_2 for Trp_9, 288°/263 − 22°; χ_1/χ_2 for Trp_{15}, 302°/264 − 19°. (B) χ_1/χ_2 for Trp_9, 288°/263 − 22°; χ_1/χ_2 for Trp_{15}, 302°/264 + 19°. Clearly, there is considerable van der Waals contact at the librational extremes when the motions are not coherent.

This has reintroduced the possibility of correlated motions or helical librations (Venkatachalam & Urry, 1984) that facilitate cation conductance by the channel or passage of cation by way of a permion (Elber et al., 1995). It is also known that the tryptophan side chains play an important role in the conductance of cations (Bamberg et al., 1976; Heitz et al., 1982; Becker et al., 1991). This role is now shown to be precisely correlated with the substantial dipole moment of the indole ring (Hu et al., 1993; Hu & Cross, 1995). The importance of the fluctuations of these dipole moments resulting from the molecular dynamics is not clear, but such motions might provide a gate for cation passage. Trp_9 and Trp_{15} have the smallest librational amplitudes, suggesting additional constraints on these two rings such as would be achieved if the two rings were stacked. Moreover, the librational motions for these two sites may be correlated and not independent as would be expected for the Trp_{11} and Trp_{13} sites. The structures in Figure 13 suggest that, when the rings librate in opposition, substantial atomic overlap occurs, whereas when the rings librate in unison, there is no substantial overlap. Correlated motions of two dipole moments, if present, would generate a more significant fluctuation in the monopole−dipole interaction energy in the channel pore (Hu & Cross, 1995).

Early ^2H NMR relaxation studies of deuterated indole rings in the gramicidin channel were interpreted to yield a global correlation time for the channel state of 200 ns at 52 °C (Macdonald & Seelig, 1988). To achieve this, the librational

amplitude that averages overlapping powder patterns was assumed to be 5−15°. This estimate and all other previous estimates (Hu et al., 1993; Koeppe et al., 1994) suggested smaller amplitudes than those that have been determined here for the individual rings. For this study, the combination of single site observations and fast frozen sample preparations has resulted in a more accurate determination of these amplitudes. Not only have librational amplitudes been determined here, but the axis about which the local motion occurs has been defined. Without such a detailed understanding of dynamics, it is not possible to accurately define the structure.

The orientation of the indole rings is uniquely defined with respect to the channel axis. Each indole is oriented with the $N_{\epsilon 1}$−H bond and the indole five-membered ring toward the bilayer surface and with the six-membered, hydrophobic ring so as to be more buried in the lipid bilayer. Here, these orientations are dynamically refined, resulting in adjustments of the torsion angles by 5−11° compared to the previous characterization (Hu et al., 1993). Furthermore, data are presented to resolve the assignment ambiguity for Trp_9 (Hu et al., 1993;Koeppe et al., 1994, 1995; Lomize et al., 1992). Through additional evidence for this assignment based on functional studies, a most probable orientation for each of the indoles will be presented in the accompanying paper (Hu & Cross, 1995). Only with such accurate orientational information is it possible to make a quantitative analysis of the dipole−monopole electrostatic interactions presented in the accompanying paper (Hu & Cross, 1995).

ACKNOWLEDGMENT

We are deeply indebted to the staff of the FSU NMR Facility, J. Vaughn, R. Rosanske, and T. Gedris, for their skillful maintenance of the facility and spectrometers and to the staff of the Bioanalytical Synthesis and Services Facility, H. Henricks and U. Goli, for their expertise and maintenance of the ABI 430A peptide synthesizer and HPLC equipment.

REFERENCES

Arumugam, S., Pascal, S., North, C. L., Hu, W., Lee, K.-C., Cotten, M., Ketchem, R. R., Xu, F., Brenneman, M., Kovacs, F., Tian, F., Wang, A., Huo, S., & Cross, T.A. (1995) *Proc. Natl. Acad. Sci. U.S.A.* (submitted for publication).

Bamberg, E., Noda, K., Gross, E., & Lauger, P. (1976) *Biochim. Biophys. Acta 419*, 223−228.

Becker, M. D., Greathouse, D. V., Koeppe, R. E., II, & Andersen, O. S. (1991) *Biochemistry 30*, 8830−8839.

Cornell, B. A., Separovic, F., & Smith, R. (1988) in *Transport Through Membranes: Carriers, Channels & Pumps* (Pullman, A., et al., Eds.) pp 289−295, Kluwer Academic Publishers, Dordrecht.

Cross, T. A. (1994) *Annu. Rep. NMR Spectrosc. 29,* 123−167.

Cross, T. A., & Opella, S. J. (1994) *Curr. Opin. Struct. Biol. 4,* 574−581.

Elber, R., Chen, D. P., Rojewska, D., & Eisenberg, R. (1995) *Biophys. J. 68,* 906−924.

Evans, J. N. S., Appleyard, R. J., & Shuttleworth, W. A. (1993) *J. Am. Chem. Soc. 115,* 1588−1590.

Fields, C. G., Fields, G. B., Noble, R. L., & Cross, T. A. (1989) *Int. J. Pept. Protein Res. 33,* 298−303.

Fields, G. B., Fields, C. G., Petefish, J., Van Wart, H. E., & Cross, T. A. (1988) *Proc. Natl. Acad. Sci. U.S.A. 85,* 1384−1388.

Frey, M. H., DiVerdi, J. A., & Opella, S. J. (1985) *J. Am. Chem. Soc. 107,* 7311−7315.

Gall, C. M., Cross, T. A., DiVerdi, J. A., & Opella, S. J. (1982) *Proc. Natl. Acad. Sci. U.S.A. 79,* 101−105.

Heitz, F., Spach, G., & Trudelle, Y. (1982) *Biophys. J. 39,* 87−89.

Hiyama, Y., Niu, C.-H., Silverton, J. V., Bavoso, A., & Torchia, D. A. (1988) *J. Am. Chem. Soc. 110,* 2378−2383.

Hu, W., & Cross, T. A. (1995) *Biochemistry 34,* 14147−14155.

Hu, W., Lee, K.-C., & Cross, T. A. (1993) *Biochemistry 32,* 7035−7047.

Ketchem, R. R., Hu, W., & Cross, T. A. (1993) *Science 261,* 1457−1460.

Killian, J. A., Taylor, M. J., & Koeppe, R. E., II. (1992) *Biochemistry 31,* 11283−11290.

Kinsey, R. A., Kintanar, A., & Oldfield, E. (1981) *J. Biol. Chem. 256,* 9028−9036.

Koeppe, R. E., II, Killian, J. A., & Greathouse, D. V. (1994) *Biophys. J. 66,* 14−24.

Koeppe, R. E., II, Killian, J. A., Vogt, T. C. B., de Kruijff, B., Taylor, M. J., Mattice, G. L., & Greathouse, D. V. (1995) *Biochemistry 34,* 9299−9306.

Lazo, N. D., Hu, W., Lee, K.-C., & Cross, T. A. (1993) *Biochem. Biophys. Res. Commun. 197,* 904−909.

Lazo, N. D., Hu, W., & Cross, T. A. (1995) *J. Magn. Reson. 107B,* 43−50.

Lee, K. C., Hu, W., Cross, T. A. (1993) *Biophys. J. 65,* 1162−1167.

Lipari, G., & Szabo, A. (1981) *J. Chem. Phys. 75,* 2971−2976.

Lomize, A. L., Orechov, V. Yu., & Arseniev, A. S. (1992) *Bioorg. Khim. 18,* 182−200.

London, R. E. (1980) in *Magnetic Resonance in Biology* (Cohen, J. S., Ed.) Vol. 1, Chapter 1, Wiley, New York.

Macdonald, P. M., & Seelig, J. (1988) *Biochemistry 27,* 2357−2364.

Nicholson, L. K., & Cross, T. A. (1989) *Biochemistry 28,* 9379−9385.

Nicholson, L. K., Teng, Q., & Cross, T. A. (1991) *J. Mol. Biol. 218,* 621−637.

North, C. L., & Cross, T. A. (1993) *J. Magn. Reson. 101B,* 35−43.

North, C. L., & Cross, T. A. (1995) *Biochemistry 34,* 5883−5895.

Separovic, F., Hayamizu, K., Smith, R., & Cornell, B. A. (1991) *Chem. Phys. Lett. 181,* 157−162.

Subramanian, E., & Sahayamary, J. J. (1989) *Int. J. Pept. Protein Res. 34,* 134−138.

Takeuchi, H., Nemoto, Y., & Harada, I. (1990) *Biochemistry 29,* 1572−1579.

Teng, Q., Iqbal, M., & Cross, T. A. (1992) *J. Am. Chem. Soc. 114,* 5312−5321.

Torchia, D. A. (1984) *Annu. Rev. Biophys. Bioeng. 13,* 124−144.

Urry, D. W. (1971) *Proc. Natl. Acad. Sci. U.S.A. 68,* 672−676.

Venkatachalam, C. M., & Urry, D. W. (1984) *J. Comput. Chem. 5,* 64−71.

Zhang, Z., Pascal, S. M., & Cross, T. A. (1992) *Biochemistry 31,* 8822−8828.

BI951624Y